scientific reports

OPEN

# Experimental study on the mechanical properties of short-cut basalt fiber reinforced concrete under large eccentric compression

Xinzhong Wang[1], Linshu Li[1], Mei Wei[2], Yi Xiang[1], Yuexing Wu[1]✉, Biao Zhou[1], Yuwen Sun[1] & Weidong Cheng[1]

**This study investigates the impact of basalt fiber on the mechanical properties of reinforced concrete members, with a specific focus on their behavior under large eccentric compression. A series of large eccentric compression tests were conducted on basalt fiber-reinforced concrete (BFRC) members with varying parameters. The failure characteristics, ultimate bearing capacity, cracking load, crack width, and other relevant factors were thoroughly analyzed. The results indicate that the mechanical properties of BFRC components are significantly improved compared to traditional concrete using basalt fiber reinforced concrete. Specifically, the ultimate bearing capacity increased by up to 30.3%, while the cracking load exhibit ed a notable increase of up to 42.9%. Notably, BFRC members displayed enhanced loading characteristics, including delayed crack initiation, a greater number of cracks, and a smaller maximum crack width. A comprehensive data simulation was performed, leading to the development of a calculation formula for the maximum crack width of BFRC members under large eccentric compression.**

**Keywords** Basalt fiber reinforced concrete column, Large eccentric compression, Mechanical properties, Cracking

Basalt Fiber Reinforced Concrete (BFRC) is a composite material in which basalt fibers are incorporated into the concrete matrix as reinforcement. This enhances the internal structure of the concrete through physical and mechanical interactions, while preserving the chemical properties of the individual constituents of the concrete[1–4]. Basalt fibers are known for their high chemical stability, thermal stability, excellent dispersion, and outstanding mechanical properties[5–7]. The addition of basalt fibers significantly improves the crack resistance, corrosion resistance, energy dissipation capacity, and overall durability and load-bearing capacity of concrete structures[8–10].

Most research on the mechanical properties of BFRC has focused on bending members. For instance, Sawalet et al.[11] concluded that the incorporation of basalt fibers does not drastically alter the fundamental mechanical properties of reinforced concrete beams. Liu et al.[12] found that adding a small quantity of short basalt fibers can reduce crack width, increase the number of cracks, delay crack propagation, improve the short-term stiffness of concrete beams, and mitigate deflection during service. Studies by Li et al.[13] and Hassan et al.[14] demonstrated that basalt fibers effectively prevent crack propagation in reinforced concrete bending members, improving the bending stiffness of concrete beams. During the elastic phase, basalt fibers have minimal impact on mid-span deflection. However, in the cracked phase, they enhance the stiffness of the beams, reducing mid-span deflection. At ultimate failure, BFRC beams exhibited greater deflection compared to conventional concrete beams.

Research on the compressive mechanical properties of BFRC is relatively limited. Wang et al.[15] performed axial compression tests on short reinforced basalt fiber concrete columns and found that basalt fibers enhanced the ultimate bearing capacity of reinforced concrete short columns. Similarly, Xue He[16] conducted eccentric compression tests on high-strength basalt fiber concrete columns, concluding that basalt fibers improved the ductility of eccentrically loaded columns.

In conclusion, basalt fibers significantly improve the mechanical properties of concrete components, providing robust strengthening and toughening effects. They are particularly effective in enhancing crack resistance in reinforced concrete bending members. However, current research predominantly focuses on pure bending or

[1]College of Civil Engineering, Hunan City University, Yiyang 413000, Hunan, China. [2]Hunan Arts And Crafts Vocational College, Yiyang 413000, Hunan, China. ✉email: wuyuexing@hncu.edu.cn

| Target strength | Water–cement ratio | Sand content (%) | Cement (kg/m$^3$) | Water (kg/m$^3$) | Sand (kg/m$^3$) | Coarse aggregate (kg/m$^3$) |
|---|---|---|---|---|---|---|
| C30 | 0.55 | 34 | 355 | 195 | 703 | 1147 |

**Table 1**. The mix proportion data.


(a) (b)

**Fig. 1**. Two lengths of basalt fiber: (**a**) L = 12 mm; (**b**) L = 24 mm.

axial compression components, with limited studies on the mechanical properties of BFRC under large eccentric compression. This study, therefore, aims to conduct experimental tests on the mechanical performance of basalt fiber concrete columns under large eccentric compression, investigating their bearing capacity, displacement characteristics, and crack development patterns.

## Experimental materials and mix proportion design
### Experimental materials
The cement used in this study was Ordinary Portland Cement (P.O. 42.5), conforming to the relevant standards. The coarse aggregates were composed of two fractions, 5–10 mm and 10–25 mm, which were blended in a ratio of 2:3 to achieve a continuous grading system. The aggregates had a crushing value of 10.5. The fine aggregate had a fineness modulus of 2.85. Potable water was used for mixing, with no water-reducing agents incorporated. The detailed mix proportions are presented in Table 1.

The basalt fibers utilized in this study were sourced from Zhejiang Hengdian Shijin Basalt Fiber Co., Ltd. The specific properties of the basalt fibers are as follows: a diameter of 17 μm, density of 26 kg·m$^{-2}$, tensile strength of 3000 MPa, and an elastic modulus of 90 GPa. The fiber lengths selected for the experiment were 12 mm and 24 mm.

To determine the optimal dosage of basalt fiber, two fiber lengths were studied: 12 mm and 24 mm (see Fig. 1). The fiber volume content in the concrete was varied across the following levels: 0%, 0.075%, 0.1%, 0.15%, 0.2%, 0.25%, 0.3%, and 0.4%. A total of 48 specimen sets were prepared, with 3 specimens per set, yielding a total of 144 specimens. Compressive strength tests were performed in accordance with GB/T 50,081 – 2002, Standard for Testing the Mechanical Properties of Ordinary Concrete. The test results are shown in Fig. 2.

From the results, it was observed that the optimal fiber volume content for basalt fibers in concrete is 0.15%. Accordingly, for the small eccentric compression column tests, the basalt fiber volume content was fixed at 0.15% throughout the study.

### Specimen design
The experimental program involves 9 large eccentric compression columns, consisting of 3 Reinforced Concrete (RC) columns and 6 Basalt Fiber Reinforced Concrete (BFRC) columns. For the BFRC columns, 3 specimens each were tested for two different fiber lengths: 12 mm and 24 mm. The basalt fiber volume content in all BFRC eccentric compression columns was uniformly set to 0.15%. The cross-sectional dimensions of all experimental columns were kept constant. Detailed dimensions of the experimental columns are presented in Fig. 3.

The loading process was carried out using a step-by-step incremental method. Initially, before the eccentric compression column developed cracks, a load increment of 10 kN was applied at each step. Once cracking was observed, the load increment was reduced to 5 kN per step. Each loading stage was maintained for 1 min until failure occurred. The large eccentric compression columns were subjected to an eccentric distance of 60 mm. A backside view of the failure of the experimental column is presented in Fig. 4.

## Failure modes
### Experimental phenomena
BF-0-0-1 Test Column: The first transverse crack appeared in the tensile zone when the load reached 45 kN, located near the lower side of the column's midsection. As the load increased, multiple cracks formed, with a

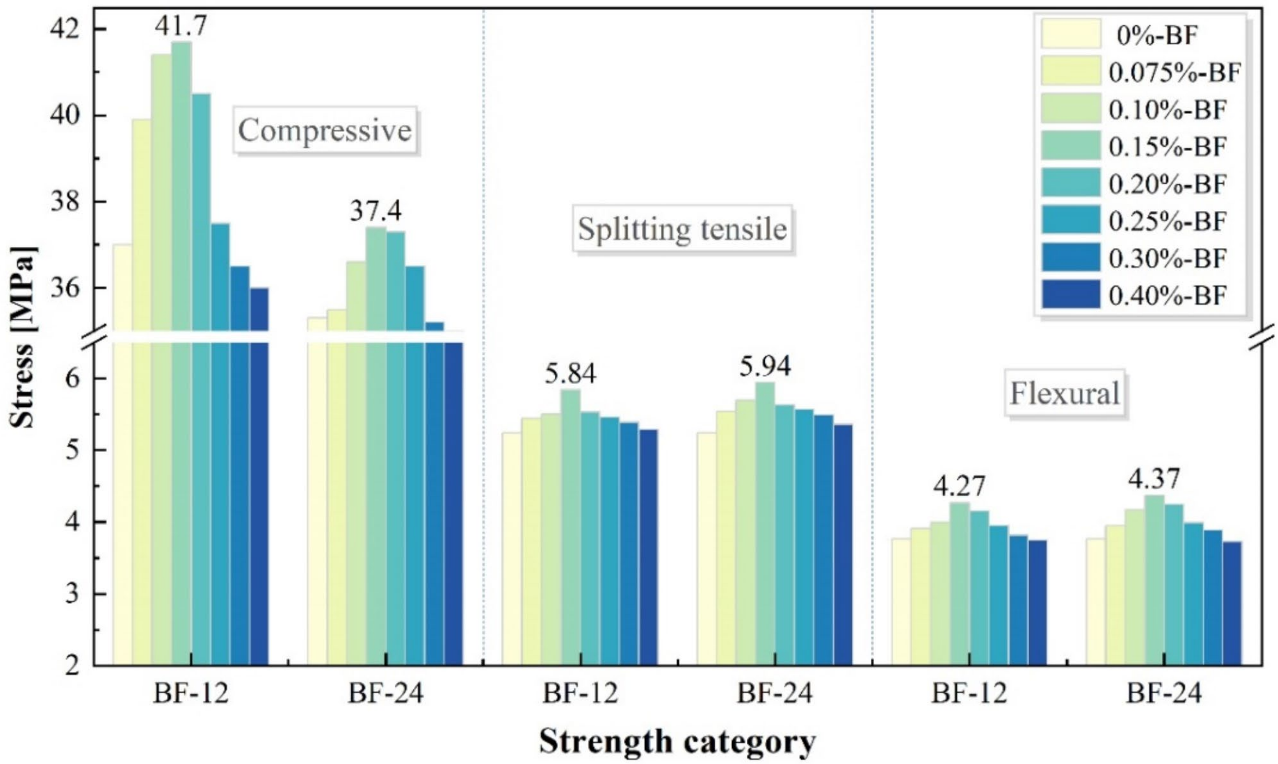


**Fig. 2**. Concrete strength at different fiber dosages.

maximum of 9 cracks spaced 7–8 cm apart. When the load reached 125 kN, the reinforcement in the tensile zone yielded, and the concrete in the compression zone was crushed, leading to the failure of the test column. BF-0-0-2 Test Column: The first transverse crack appeared in the tensile zone when the load reached 40 kN. As the load increased, multiple cracks formed, with a maximum of 7 cracks spaced 7–8 cm apart. When the load reached 115 kN, the reinforcement in the tensile zone yielded, and the concrete in the compression zone was crushed, leading to the failure of the test column.BF-0-0-3 Test Column: The first transverse crack appeared in the tensile zone when the load reached 40 kN, with a maximum of 7 cracks. The test column failed when the load reached 125 kN.

BF-12-0.15-1 Test Column: The first transverse crack appeared in the tensile zone when the load reached 55 kN. As the load increased, a maximum of 8 cracks formed, with a crack spacing of 6–7 cm. When the load reached 135 kN, the reinforcement in the tensile zone yielded, and the concrete in the compression zone was crushed, leading to the failure of the test column.BF-12-0.15-2 Test Column: The first transverse crack appeared in the tensile zone when the load reached 60 kN. As the load increased, a maximum of 9 cracks formed, with a crack spacing of 6–7 cm. When the load reached 130 kN, the reinforcement in the tensile zone yielded, and the concrete in the compression zone was crushed, leading to the failure of the test column.BF-12-0.15-3 Test Column: The first transverse crack appeared in the tensile zone when the load reached 60 kN. As the load increased, a maximum of 9 cracks formed, with a crack spacing of 6–7 cm. When the load reached 130 kN, the reinforcement in the tensile zone yielded, and the concrete in the compression zone was crushed, leading to the failure of the test column.

BF-24-0.15-1 Test Column: The first transverse crack appeared in the tensile zone when the load reached 60 kN. As the load increased, a maximum of 9 cracks formed, with a crack spacing of 5–6 cm. When the load reached 160 kN, the reinforcement in the tensile zone yielded, and the concrete in the compression zone was crushed, leading to the failure of the test column.BF-24-0.15-2 Test Column: The first transverse crack appeared in the tensile zone when the load reached 70 kN. As the load increased, a maximum of 10 cracks formed, with a crack spacing of 5–6 cm. When the load reached 160 kN, the reinforcement in the tensile zone yielded, and the concrete in the compression zone was crushed, leading to the failure of the test column.BF-24-0.15-3 Test Column: The first transverse crack appeared in the tensile zone when the load reached 60 kN. As the load increased, a maximum of 8 cracks formed, with a crack spacing of 5–6 cm. When the load reached 165 kN, the reinforcement in the tensile zone yielded, and the concrete in the compression zone was crushed, leading to the failure of the test column.

### Typical failure modes

For all three test columns, the first transverse crack appeared in the tensile zone near the lower side of the column's mid-section as the applied load reached the cracking point. As loading continued, multiple cracks

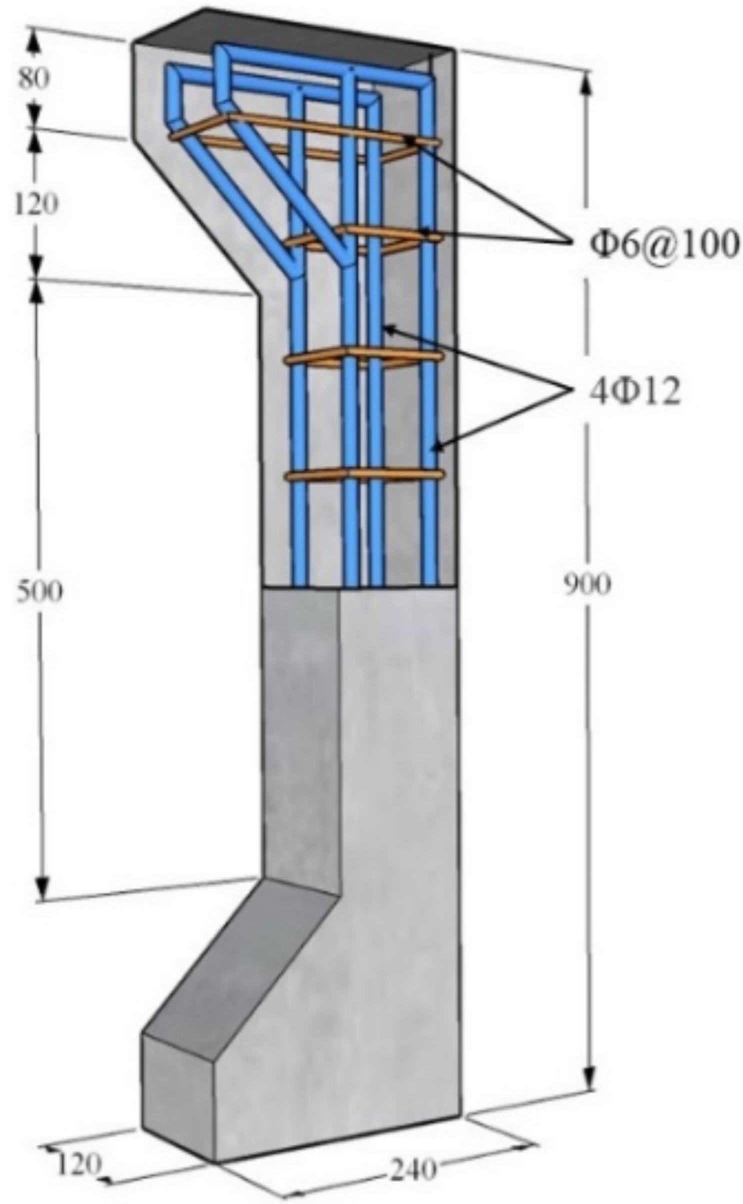


**Fig. 3**. Detailed structural dimensions of the experimental columns (unit: mm).

developed sequentially. In the case of RC (Reinforced Concrete) columns under large eccentric compression, once horizontal cracks appeared in the tensile zone, they rapidly propagated and widened. This progression caused the concrete in the tensile zone to no longer participate in the load-bearing process effectively. The strain in the compressed zone of the concrete quickly reached its ultimate compressive strain, leading to the crushing and peeling off of the protective layer. After failure, the overall integrity of the RC specimen was compromised, and the column's load-bearing capacity was severely diminished.

In contrast, the BFRC (Basalt Fiber Reinforced Concrete) columns demonstrated notable improvements in failure behavior. The incorporation of basalt fibers provided enhanced crack control through their toughening and crack-bridging properties. In the BFRC eccentric compression columns, the crack spacing in the tensile zone was smaller, crack propagation was significantly slower compared to the RC columns, and the crack width was notably reduced. These characteristics indicate that the basalt fibers played a crucial role in improving the overall structural performance, enhancing durability, and delaying the onset of complete failure.

## Experimental results and analysis
### Ultimate load capacity
The measured cracking load and ultimate load values for each test column are summarized in Table 2. The results clearly indicate that the ultimate load capacity of BFRC (Basalt Fiber Reinforced Concrete) columns subjected to large eccentric compression is significantly higher than that of RC (Reinforced Concrete) columns. Specifically,

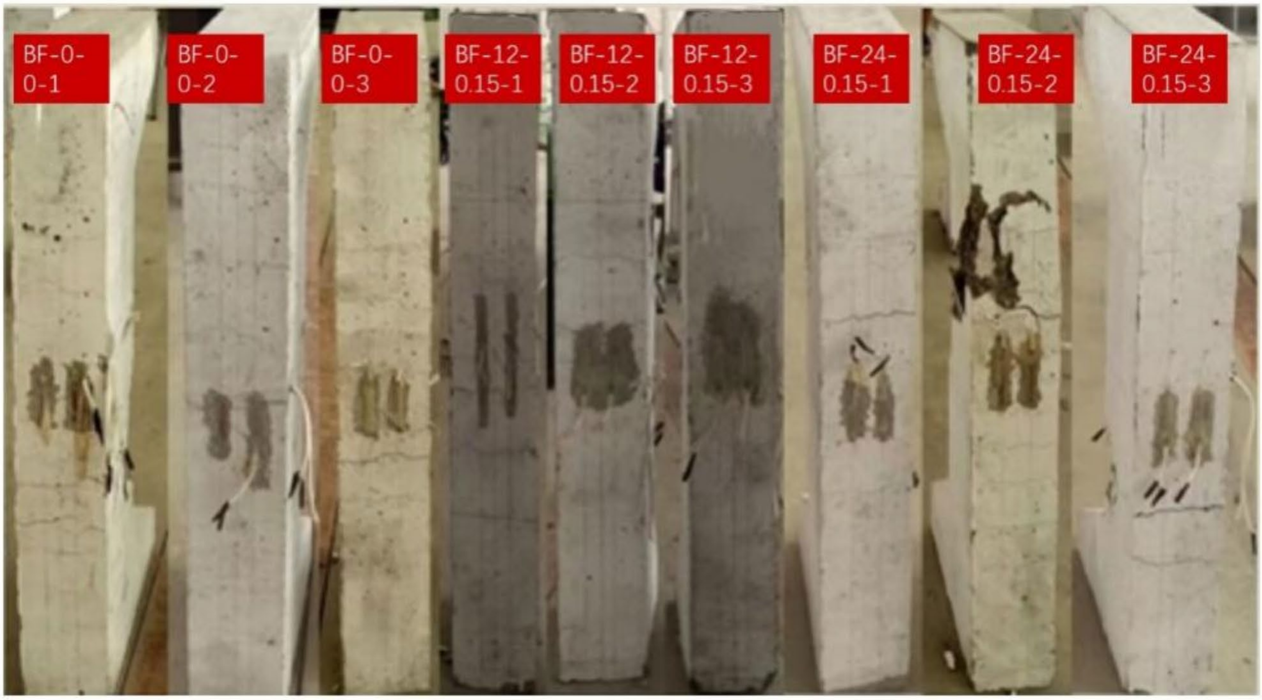


**Fig. 4**. Backside view of the failure of the large eccentric compression reinforced concrete column.

| Large eccentric compression column ID | Cracking load (kN) | Ultimate load (kN) | Peak lateral displacement | Maximum crack width |
|---|---|---|---|---|
| BF-0-0-1 | 45 | 125 | 4.78 | 0.252 |
| BF-0-0-2 | 40 | 115 | 4.81 | 0.248 |
| BF-0-0-3 | 40 | 125 | 4.82 | 0.243 |
| BF-12-0.15-1 | 55 | 135 | 5.61 | 0.222 |
| BF-12-0.15-2 | 60 | 130 | 5.32 | 0.220 |
| BF-12-0.15-3 | 65 | 130 | 5.21 | 0.216 |
| BF-24-0.15-1 | 60 | 160 | 5.75 | 0.204 |
| BF-24-0.15-2 | 70 | 160 | 5.14 | 0.206 |
| BF-24-0.15-3 | 60 | 165 | 5.81 | 0.198 |

**Table 2**. Experimental results of reinforced basalt fiber large eccentric compression members.

the load capacity of columns with 12 mm basalt fiber increased by an average of 8.0%, while columns with 24 mm basalt fiber demonstrated a more substantial increase of 24.8%.

This improvement in load-bearing capacity underscores the positive contribution of basalt fibers in enhancing the structural performance of large eccentric compression columns. Furthermore, the influence of fiber length is also evident, with the 24 mm fibers yielding a more pronounced enhancement. This effect highlights the role of basalt fiber's random distribution within the concrete matrix, which improves crack resistance and overall durability. The enhanced crack resistance is particularly evident in both bending and compression members, where the fibers help to control crack propagation and improve the material's energy dissipation capacity.

## Load-displacement curve

Figure 5 illustrates the variation in horizontal displacement at the midpoint of the large eccentric compression test columns as the load increases. The graph reveals that during the elastic working phase, the lateral deflection of the Basalt Fiber Reinforced Concrete (BFRC) columns is smaller than that of the ordinary Reinforced Concrete (RC) columns. As the load progresses, the deflection of the BFRC columns gradually increases, with the deflection of the BFRC columns at the ultimate load being slightly larger than that of the RC columns. Notably, under the ultimate load, the horizontal displacement of the BFRC columns with 24 mm basalt fibers is greater than that of the columns with 12 mm basalt fibers, suggesting that longer fiber lengths contribute to improved toughness in larger columns.During the elastic stage, the basalt fibers enhance the crack resistance and bending stiffness of the concrete, leading to reduced deflection. However, as cracks develop, the fibers' crack resistance effect diminishes, and the displacement increases gradually. This behavior is primarily attributed to

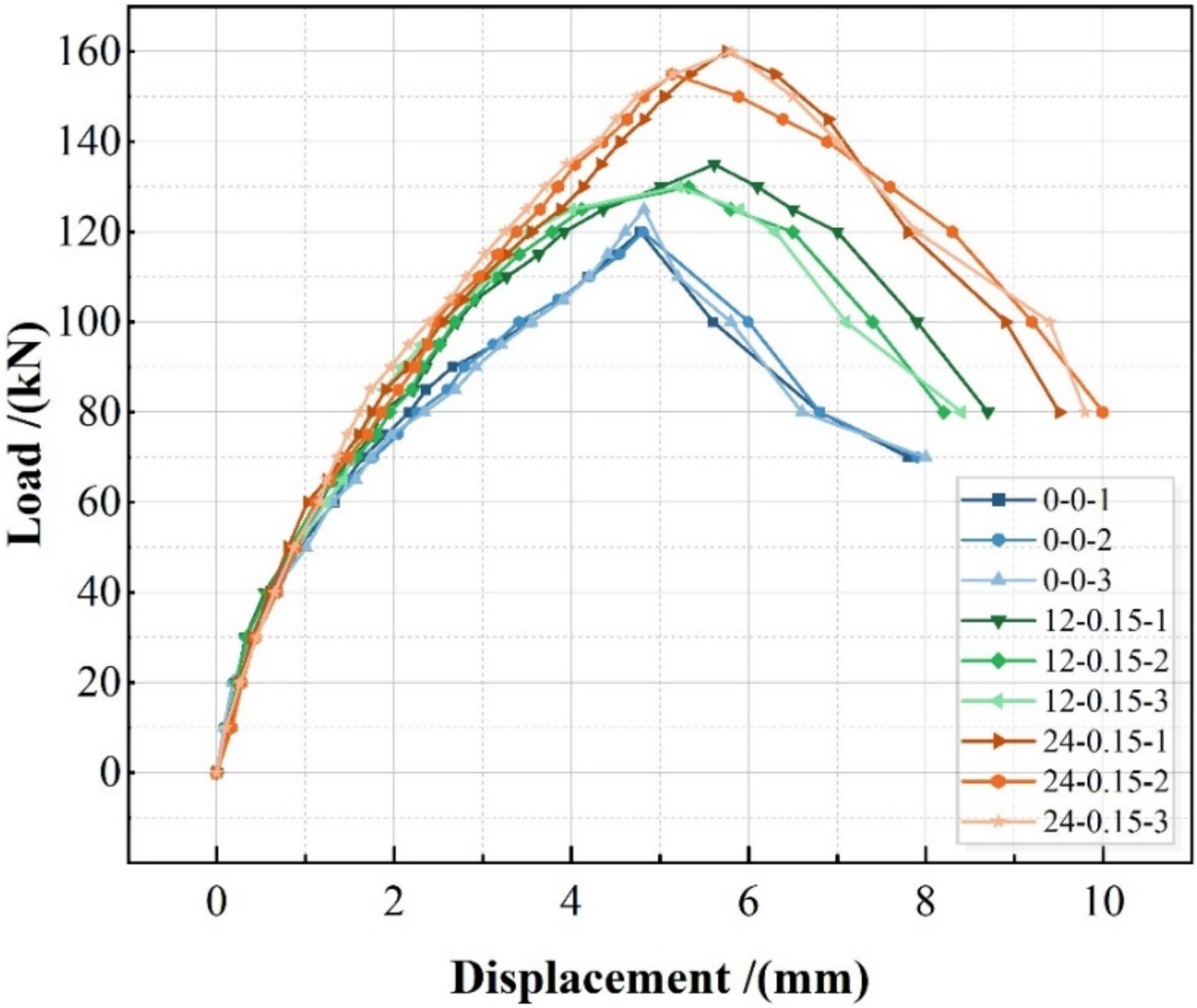


**Fig. 5**. Load vs. lateral displacement curve of large eccentric compression long column.

the basalt fibers' role in bearing a portion of the tensile stress in the concrete's tensile zone. By inhibiting the propagation of cracks and limiting crack width and extension, the fibers help preserve the load-bearing capacity of the concrete. This enables certain concrete portions, which would otherwise have lost their load-carrying ability, to maintain their stressed state, thereby improving the overall bending stiffness of the BFRC specimens.

According to references[17,18], when a rod is subjected to eccentric pressure P and bends, the deflection at any section x is v, and the bending moment at this section is:

$$M\left(x\right)=P\left(e+v\right) \tag{1}$$

The approximate differential equation for the deflection curve of the rod is:

$$EI_{z}v^{''}=-M\left(x\right)=-P\left(e+v\right) \tag{2}$$

Divide both sides of Eq. (2) by $EI_z$, and let

$$\text{Divide both sides of equation (2) by } EI_{z},\text{ and let } \frac{P}{EI_{z}}=k^{2} \tag{3}$$

Equation (2) can be rewritten as:

$$\text{Equation (2) can be rewritten as}: v^{\prime\prime}+k^{2}v=-k^{2}e \tag{4}$$

The general solution of this differential equation is:

$$\text{The general solution of this differential equation is}: v = A \sin kx + B \cos kx - e \tag{5}$$

According to the boundary conditions of the deflection curve: $x = 0, v = 0$ and $x = 1, v = 0$, From Eq. (5), the constants A and B can be determined as:

$$B = e, A = \frac{e\,(1 - \cos kl)}{\sin kl} = etg\frac{kl}{2} \tag{6}$$

Thus, the deflection curve equation of the rod under the action of eccentric load P can be written as:

$$v = e\left(tg\frac{kl}{2}\sin kx + \cos kx - 1\right) \tag{7}$$

Given that the maximum deflection $\delta$ occurs at the midpoint of the rod, i.e., at point $x = l/2$.
By substituting $x = l/2$ into (7), the expression for the maximum deflection $\delta$ can be obtained:

$$\delta = v\left|_{x=l/2} = e\left(\sec\frac{kl}{2} - 1\right)\right. \tag{8}$$

The displacement allows for the determination of value $k$, which can then be substituted into Eq. (3) to obtain value $EI_z$. The stiffness of each test column is shown in Fig. 6.

Figure 6 illustrates the variation in bending stiffness of both RC (Reinforced Concrete) and BFRC (Basalt Fiber Reinforced Concrete) columns as the load increases. Before reaching the cracking load, the RC columns exhibit higher bending stiffness, characterized by relatively small maximum deflections. This results in RC columns displaying significantly higher bending stiffness compared to BFRC columns in the initial loading

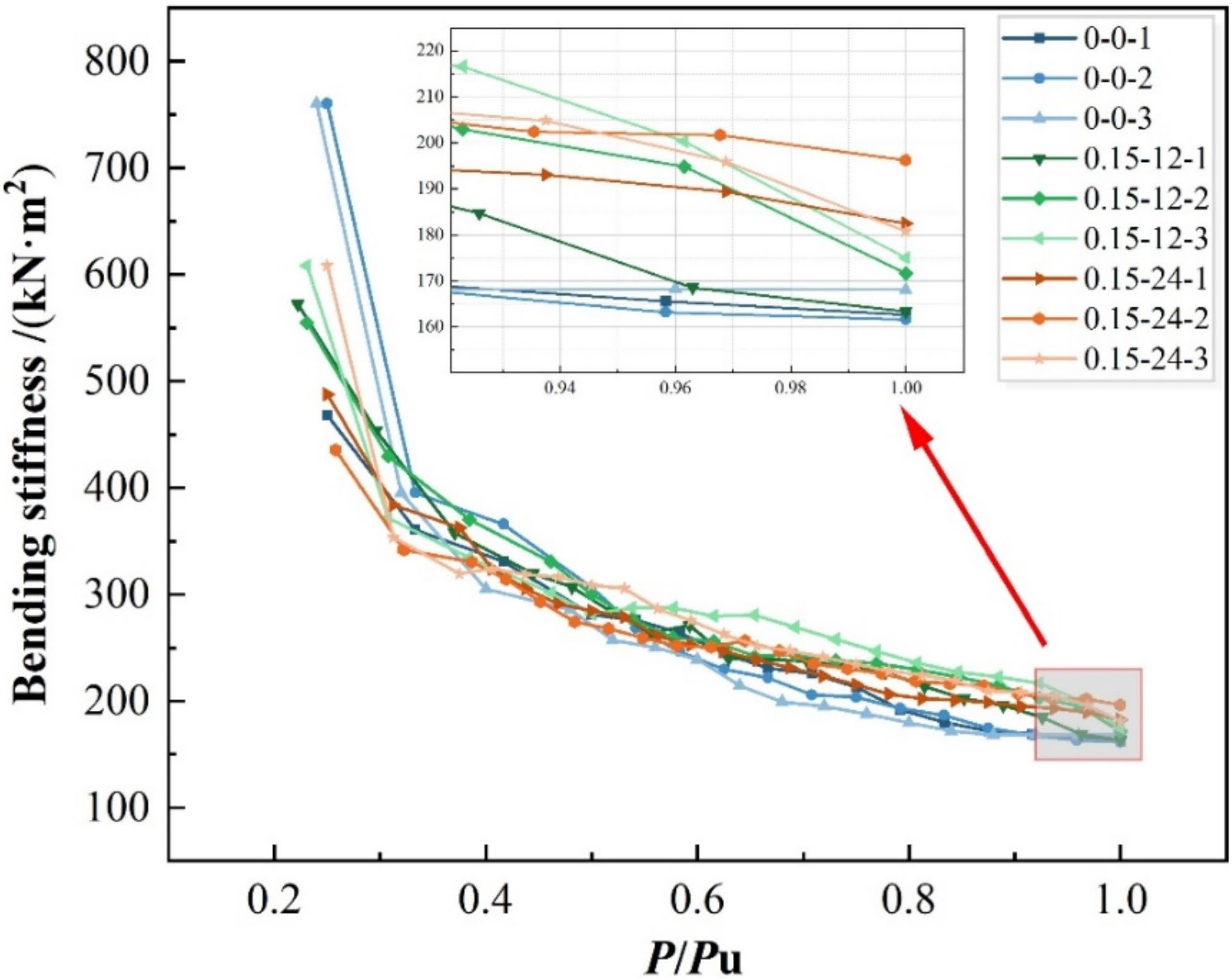


**Fig. 6**. Calculation of the equivalent stiffness value for eccentrically compressed columns with large eccentricities.

stages. As the load continues to increase, the bending stiffness of the RC columns decreases sharply. After the cracking load is reached, the bending stiffness of RC columns becomes lower than that of BFRC columns. In the subsequent crack-propagation phase, the bending stiffness of the RC columns continues to decrease without interruption, and the decline is reflected in an increasingly steeper curve.

In contrast, the bending stiffness of the BFRC columns decreases more gradually, with a gentler slope. This indicates that basalt fibers play a role in enhancing the column's resistance to bending throughout the loading process. Ultimately, at the ultimate load, the equivalent flexural stiffness of the BFRC columns is higher than that of the RC columns. Notably, BFRC columns with 12 mm basalt fibers exhibit greater equivalent flexural stiffness compared to those with 24 mm fibers, suggesting that the shorter fibers contribute more effectively to maintaining bending stiffness under large eccentric compression.

### Load-concrete strain curve

Figure 7 shows the curve of the average strain at the concrete edge in the compression zone (near the eccentric side) of the midsection of 9 large eccentricity test columns, as the load varies. From Fig. 7, it can be observed that the strain variation trends for both BFRC and RC large eccentricity compressed columns are generally consistent. Under the same load level, the compressive strain in the BFRC large eccentricity compressed columns is smaller than that in the RC large eccentricity compressed columns. However, at the ultimate load, the absolute value of the compressive strain in the BFRC large eccentricity compressed columns is greater than that in the RC large eccentricity compressed columns at their respective ultimate loads.

### Crack analysis of large eccentrically compressed columns

Figure 8 illustrates the crack patterns of the tensile face and the two lateral faces of the large eccentricity test columns after unfolding, with the numerical values representing the cracking loads (in kN). It can be observed

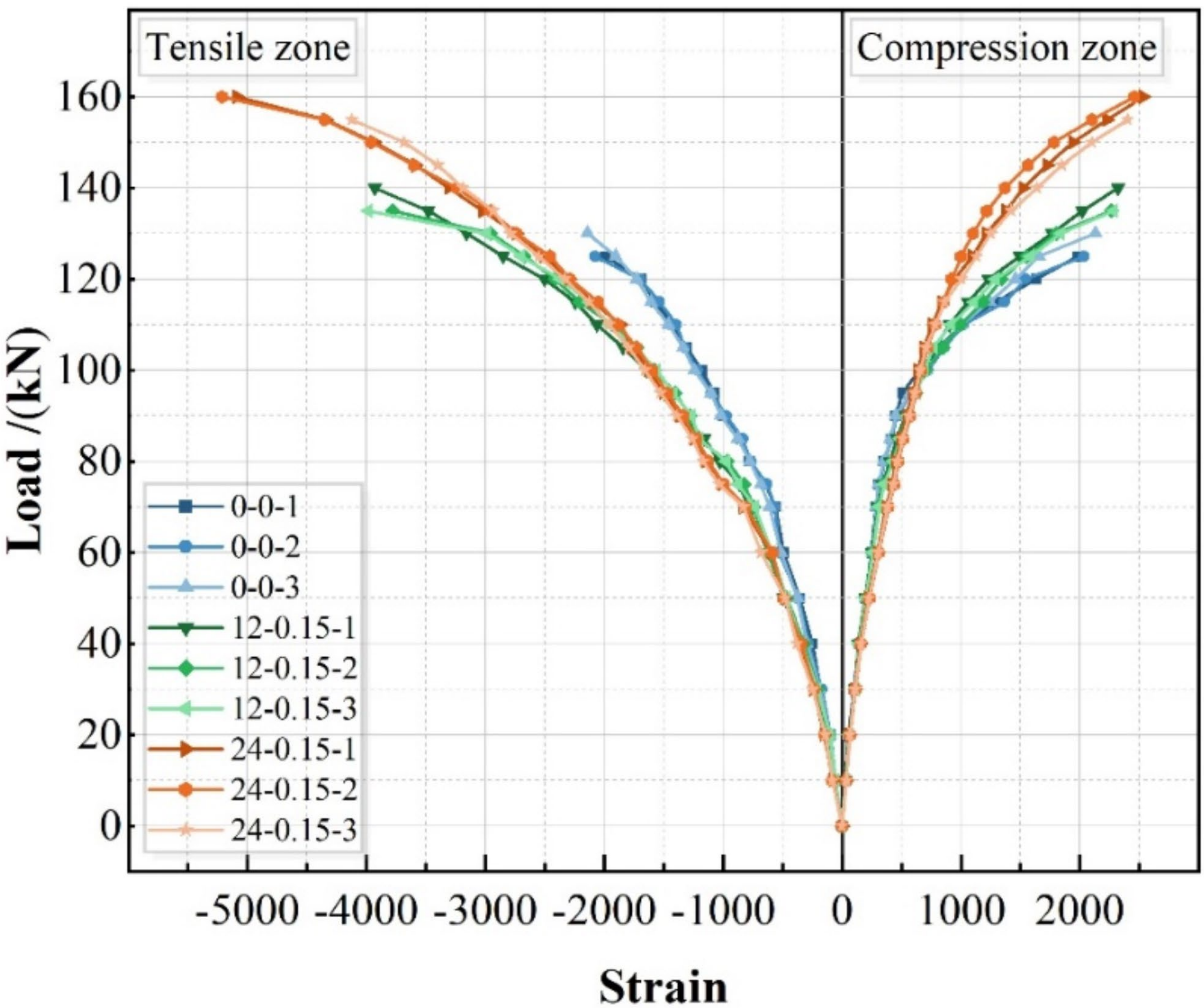


**Fig. 7**. Load-strain curve of test columns.

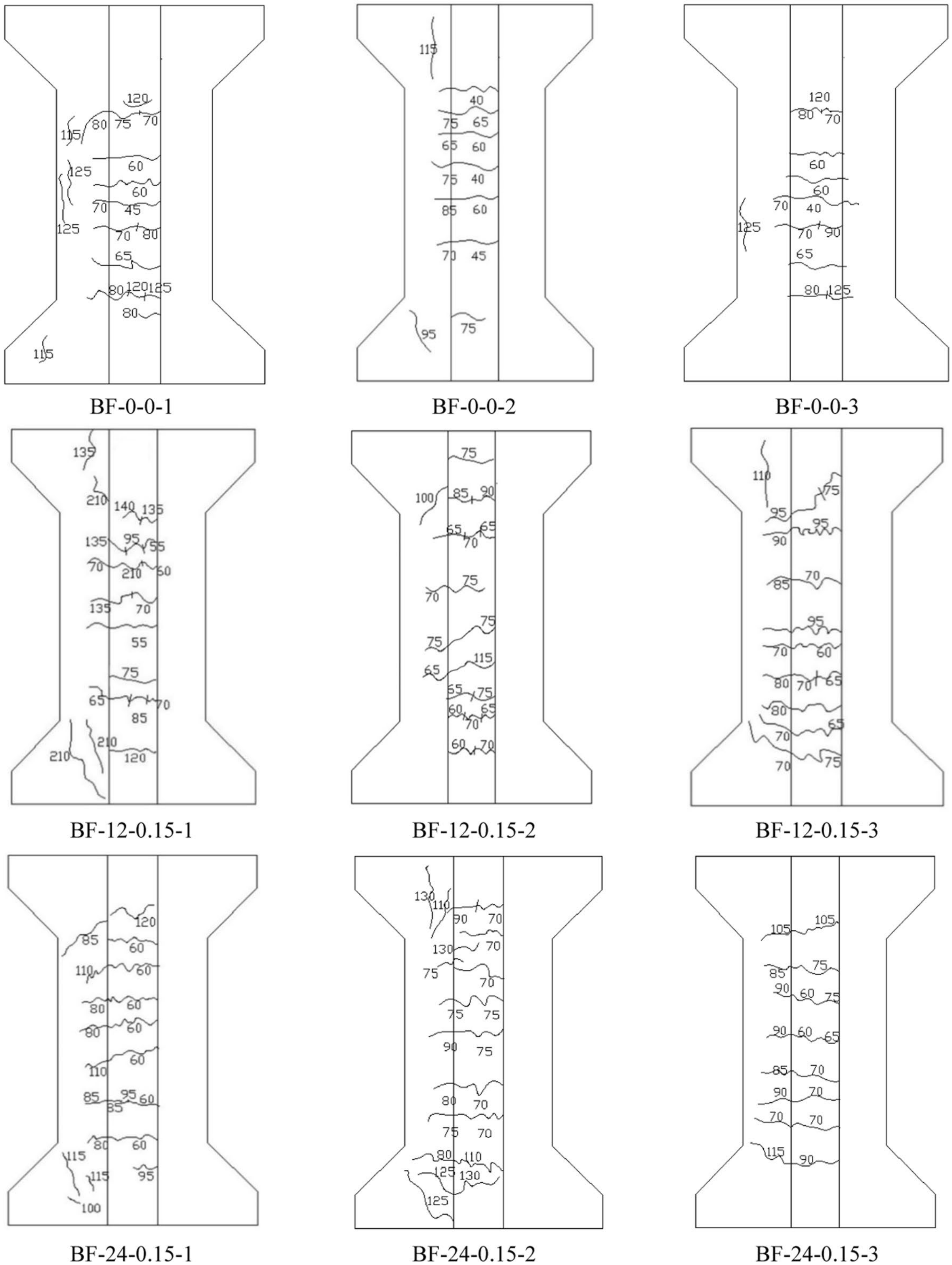


**Fig. 8**. Crack pattern of reinforced basalt fiber large eccentricity compressed members.

that, compared to the RC large eccentricity compressed columns, the BFRC large eccentricity compressed columns exhibit higher cracking loads, more cracks, and a larger distribution area of the cracks.

Before cracking, the tensile stress in the BFRC specimens is shared by both the concrete at the tensile edge and the fibers, which delays the initiation of the first crack. After the bending cracks appear, compared to ordinary concrete specimens, the vertical crack extension height in the BFRC specimens is reduced to varying degrees under the same load. This indicates that the tensile stress is jointly borne by the reinforcement, basalt fibers (BF), and a portion of the uncracked concrete, reflecting the strengthening effect of the BF on the specimens. Once

| Large eccentricity compressed column number | Eccentric (mm) | Measured maximum crack width w1 (mm) | Maximum crack width calculated by code w2 (mm) | Calculated value using formula (11) (mm) | Relative error |
|---|---|---|---|---|---|
| BF-0-0-1 | 60 | 0.252 | 0.252 | 0.252 | 0.00% |
| BF-0-0-2 | 60 | 0.248 | 0.248 | 0.248 | 0.00% |
| BF-0-0-3 | 60 | 0.243 | 0.243 | 0.243 | 0.00% |
| BF-12-0.15-1 | 60 | 0.222 | 0.236 | 0.229 | 3.06% |
| BF-12-0.15-2 | 60 | 0.220 | 0.232 | 0.225 | 2.22% |
| BF-12-0.15-3 | 60 | 0.216 | 0.23 | 0.223 | 3.14% |
| BF-24-0.15-1 | 60 | 0.204 | 0.224 | 0.210 | 2.86% |
| BF-24-0.15-2 | 60 | 0.206 | 0.226 | 0.212 | 2.83% |
| BF-24-0.15-3 | 60 | 0.198 | 0.222 | 0.208 | 4.81% |

**Table 3**. Maximum crack width values.

the bond stress between the BF and the matrix reaches the bond strength, debonding occurs, causing some fibers to be pulled out, which weakens the strengthening effect of the fibers progressively as the load increases. When the loading reaches the yielding and ultimate states, crack propagation becomes more pronounced, and the strengthening effect of the BF essentially disappears. Ultimately, the specimen fails due to the yielding of the longitudinal reinforcement and concrete crushing. At the ultimate peak load, the influence of concrete's tensile strength on crack width becomes negligible, with the crack width mainly determined by the reinforcement ratio of the reinforced concrete column.

According to the standards[19,20], the maximum crack width calculation formula for large eccentrically compressed columns is:

$$W_{\max} = C_1 C_2 C_3 \frac{\sigma_{ss}}{E_s} \left( \frac{30 + d}{0.28 + 10\rho} \right) \tag{9}$$

$$\rho = \frac{A_S}{bh_0} \tag{10}$$

For plain round steel bars,$C_1 = 1.4$, for ribbed steel bars, $C_2 = 1.0$, $C_3 = 0.9$

$\sigma_{ss}$ Rebar Stress $\rho$ Longitudinal Tensile Reinforcement Ratio, $\rho$ If greater than 0.02, take 0.02; if less than 0.006, take 0.006.

The measured and calculated crack values for the large eccentricity test columns are shown in Table 3. It can be observed that the cracks in the BFRC large eccentricity compressed columns are smaller than those in the RC large eccentricity compressed columns.

This paper uses the calculation model from reference[21] and, through linear regression of the coefficient, provides the formula for calculating the maximum crack width of basalt fiber reinforced concrete large eccentricity compressed square columns, as follows:

$$\omega_{f\,\max} = \omega_{\max}(1 - \beta_{bcw}\lambda_f) \tag{11}$$

In the formula, $\omega_f\max$ represents the maximum crack width of the basalt fiber reinforced concrete beam; $\beta_{bcw}$ is the coefficient that accounts for the influence of basalt fiber incorporation on the crack width of the member. Linear regression of the data yields $\beta_{bcw} = 0.0975$, which is simplified to 0.1 for calculation purposes. $\lambda_f$ (aspect ratio) is a characteristic parameter of the basalt fiber. Using formula (11), the maximum crack width of the test column cross-section is verified, and the comparison results are shown in Table 3. As seen in Table 3, the measured maximum crack width of the test column cross-section closely matches the calculated values.

## Conclusion

This paper presents the results of an eccentric compression test on reinforced basalt fiber concrete (BFRC) square columns, utilizing two different fiber lengths. Through the analysis of experimental phenomena and results, the following conclusions can be drawn:

- The incorporation of basalt fiber significantly enhances the mechanical performance of large eccentricity compressed concrete columns. The crack-arresting and toughening effects of basalt fibers lead to a notable increase in the cracking load of BFRC columns compared to RC columns. Specifically, the cracking load of BFRC columns with 12 mm fiber length increases by an average of 30.6%, while the cracking load of BFRC columns with 24 mm fiber length increases by an average of 34.2%, with the maximum observed increase reaching 42.9%;
- The ultimate load capacity of concrete columns also increases with the incorporation of basalt fibers. On average, BFRC columns exhibit a 30.3% increase in ultimate load compared to RC columns. Additionally, as the fiber length increases, the ultimate load capacity improves further, with 12 mm fibers contributing to a 5.2% increase, and 24 mm fibers resulting in a 24.7% increase in ultimate load.

- Upon reaching the cracking load, BFRC columns exhibit smaller crack widths compared to RC columns. During subsequent loading, the toughening and crack-arresting properties of the basalt fibers enable better crack control in BFRC columns. These columns show more cracks, but with smaller widths, compared to RC columns, which develop fewer, wider cracks and are more prone to failure.
- A comparison of the maximum crack widths predicted by the code formula, the modified formula introduced in this study, and the measured experimental values shows a high degree of consistency. This suggests that the code formula is effective to some extent, while the modified formula provides a more accurate reflection of actual conditions. This validates the modified formula as a reliable tool for structural design and evaluation of concrete columns.

## Data availability
All data generated or analysed during this study are included in this published article.

Received: 3 December 2024; Accepted: 18 March 2025
Published online: 29 March 2025

## References
1. Li, W. et al. Strengthening and toughening in basalt fiber-reinforced concrete. *J. Chin. Ceramic Soc.* **36**(4), 476–481 (2008).
2. Zhu, F.F. et al. Freeze–thaw test and numerical analysis of basalt reinforced fiber concrete in Western saline soil area. *J. Chin. Ceramic Soc.* **52**(11), 3431–3443 (2024).
3. Yang, Y.M. et al. Machine learning-based probabilistic prediction model for chloride concentration in the interfacial zone of precast and cast-in-place concrete structures. Structures, **72**, 108224 (2025).
4. Guo, Y.D. et al. Influence of basalt fiber characteristic parameters on uniaxial tensile properties of concrete. *Acta Materiae Compositae Sinica*, **40**(5), 2897–2912 (2023).
5. Ping, H. & Xianghua, S. Optimizing fiber-reinforced flexible concrete blankets: A study on basalt fiber effects on strength properties. *Constr. Build. Mater.* **456**, 139272 (2024).
6. Yang, Q.G. et al. Prediction of mechanical properties of basalt fiber concrete using hybrid recurrent neural networks based on freeze-thaw damage quantification. *J. Building Eng.*, 111360 (2024).
7. Yang, Y.M. et al. Theory-informed deep neural network-based time-dependent flexural reliability assessment of corroded PC structures. Engineering Structures, **329**, 119819 (2025).
8. Zhang, Z., Zhang, K. & Gong, D. Experimental study on low temperature mechanical properties of basalt fiber concrete under impact load. *Compos. Sci. Eng.* (9), 36–41 (2023).
9. Tang, H. et al. Test and Theoretical Investigations on Flexural Behavior of High-Performance H-Shaped Steel Beam with Local Corrosion in Pure Bending Zone[J]. steel research international, 2400640 (2024).
10. Wu, Y.X. et al. Research on the cross-sectional geometric parameters and rigid skeleton length of reinforced concrete arch bridges: A case study of Yelanghu Bridge. Structures. **69**, 107423 (2024).
11. Sawulet·Bekey, D. et al. Experimental study on flexural behavior of basalt fibers admixing desert sand Rc beam. *Building Struct.* **54**(18), 131–135 (2024).
12. Liu, Q. et al. Experimental study on flexural behavior of normal section of simply-supported chopped basalt fiber-reinforced concrete beams. *J. Building Struct.* **43**(12), 189–198 (2022).
13. Li, S. et al. Flexural behaviour of post-tensioned precast beams manufactured with basalt-fibre-reinforced recycled concrete–conventional concrete. *J. Building Eng.* **89**, 109154 (2024).
14. Hassan, B. R. & Yousif, A. R. Shear performance and strength of reinforced concrete non-prismatic beams with basalt fiber reinforced polymer rebars. *Structures* **65**, 106571 (2024).
15. Wang, X.Z. et al. Experimental analysis of bearing capacity of basalt fiber reinforced concrete short columns under axial compression. *Coatings* **12**(5), 654 (2022).
16. Xue, H. *Experimentai Study on Basalt fiber High Strength Concrete Under Eccentric compression* (Northeast Forestry University, 2019).
17. Fan, T. et al. Code for Design of Concrete Structures. (Chongqing University, 2017).
18. Ye, J. *Priciples of Structural design* (China Communication, 2018).
19. JTG 3362 – 2018. *Code Design of Highway Reinforced Concrete and Prestressed Concrete Bridges and culverts* 30–40 (China Communication, 2018).
20. CECS38-2004. *Technical Specification for fiber Reinforced Concrete Structures* (China Planning, 2004).
21. Wang, J. et al. Experimental research on crack and deformation of basalt fiber reinforced concrete beams. *J. Archit. Civil Eng.* **33**(4), 76–81 (2016).

## Acknowledgements
This work was supported by the Natural Science Foundation of Hunan Province, China (2024JJ7170 and 2024JJ7077); the Research Foundation of Education Bureau of Hunan Province, China (22A0561, 23B0732 and 23A0559); the Research Foundation of Graduate Research Innovation of Hunan Province, China (CX20240099, CX20240984, LXBZZ2024376 and LXBZZ2024379); the Research Foundation of Science and Technology Bureau of Yiyang City, China ((2023)102).

## Author contributions
All authors contributed to the study conception and design W.X.Z. and L.L.S. wrote and reviewed the manuscript; W.Y.X. and W.M. collected the data; C.W.D. and S.Y.W. complete the photo processing; Z.B. and X.Y. reviewed the manuscript.

## Declarations

## Competing interests
The authors declare no competing interests.

## Additional information

**Correspondence** and requests for materials should be addressed to Y.W.

**Reprints and permissions information** is available at www.nature.com/reprints.

**Publisher's note** Springer Nature remains neutral with regard to jurisdictional claims in published maps and institutional affiliations.